RESEARCH ARTICLE

Nanobiopesticides: Silica nanoparticles with spiky surfaces enable dual adhesion and enhanced performance

Jun Zhang[1] | Geoff Brown[2] | Jianye Fu[1] | Peter James[3] | Lillian Mukandiwa[3] | Xiaodan Huang[1] | Chengzhong Yu[1] (ORCID)

[1]Australian Institute for Bioengineering and Nanotechnology, The University of Queensland, Brisbane, Queensland, Australia

[2]Department of Agriculture and Fisheries, Agri-Science Queensland, Brisbane, Queensland, Australia

[3]Queensland Alliance for Agriculture and Food Innovation, The University of Queensland, Brisbane, Queensland, Australia

Correspondence
Chengzhong Yu, Australian Institute for Bioengineering and Nanotechnology, The University of Queensland, Brisbane, Queensland 4072, Australia.
Email: c.yu@uq.edu.au

Abstract

Biopesticides, such as spinosad, are a new-generation of ecofriendly pesticides in livestock industry. However, spinosad suffers from short duration of effectiveness and low potency in field conditions. Herein we report the development of a new nanospinosad design with dual adhesion and protection functions. Silica nanoparticles with spiky nanotopography loaded with spinosad possess rough surfaces. When applied topically, this nanospinosad formulation exhibited enhanced adhesion to both cattle hair and pest surface. The dual adhesion property led to significantly higher pest mortality toward tick (*Rhipicephalus microplus*, an ectoparasite) than a nanospinosad formulation using nanoparticles with smooth surface and a benchmark commercial product. The adhesion performance was further quantitatively measured using rainfastness test. Moreover, solar radiation test revealed that the nanospinosad exhibited >10 times higher photostability over the commercial product. This work paves the way toward the development of high performance nanobiopesticides for sustainable agricultural applications.

KEYWORDS

biopesticides, dual adhesion, mesoporous silica, pest control, silica nanoparticles

1 | INTRODUCTION

Ecofriendly biopesticides extracted from natural products provide new opportunities to combat pests/ectoparasites with low resistance and reduced environmental impact.[1-4] Spinosad is a typical biopesticide naturally derived from an actinomycete bacterium species (*Saccharopolyspora spinosa*), and has been registered for use in pest control by US Environmental Protection Agency.[5-7] Spinosad has been demonstrated highly active through both contact and ingestion to numerous pests,[6] while it shows low risk toward mammals and many aquatic or avian animals.[5,8] In laboratory conditions, spinosad was reported to be quite stable and capable of causing a high prevalence of mortality up to 1 month.[9] However, under field conditions spinosad degraded rapidly[10-12] and showed little toxicity at 3 to 7 days postapplication,[13] mainly because sunlight and rainfall

can quickly degrade and dilute spinosad. The short duration of efficacy and reduced potency have prevented spinosad as an efficient treatment for cattle ectoparasites such as ticks, which requires repeated applications, leading to high costs.[14,15] Moreover, cattle hides with relatively short fur cannot provide sufficient protection/adhesion for spinosad, resulting in serious photodegradation and poor rainfastness.[14] Up to now, it remains challenging to develop spinosad formulations with both high photostability and high rainfastness property.

Recently, nanomaterials, such as polymers,[16,17] nanocrystals,[18] lipid nanoparticles,[19,20] and nanoporous silicas,[21-23] have been employed to develop nanopesticide formulations for sustained release and enhanced efficacy. Among these nanomaterials, nanoporous silicas have unique properties including high porosity for payload, stable/rigid framework, ease of synthesis and excellent biocompatibility,[24,25] which are ideal for agriculture applications. Nanopesticide formulations using mesoporous silica monolith and mesoporous silica nanoparticles as carriers have been recently reported, showing interesting sustainable release properties.[26-30] A recent study using mesoporous silica hollow spheres to encapsulate biopesticide—avermectin—revealed that the siliceous shells could provide ultraviolet (UV) shielding effect and play as a useful protection to address the photoinduced instability issue of photolabile pesticides.[28] Nanocarriers enabled photoprotections to pesticides (eg, deltamethrin) have also been reported elsewhere.[19,20] Recently, Huang et al reported reduced sunlight degradation and sustained release of microsize polymer carrier encapsulated spinosad and emamectin benzoate on foliar substrates (cabbage leaves, *Brassica oleracea* L.),[31] while other key property, such as rainfastness, remains unclarified.

Besides sunlight radiation, rainfall is another natural factor that washes off and dilutes the veterinary pesticide actives to a sublethal level in livestock industry.[10,32-34] To maintain the fatal pesticide residue, farmers have to conventionally reapply pesticide after rainfall, which is cost/labor consuming.[35] Enhancing the adhesion of pesticides toward biological substrates is an important strategy to improve their rainfastness properties for withstanding rainfall. Previous studies using "film-forming materials" (latex or starch based binders) as adjuvants in organophosphorous pesticide formulations displayed good adhesion to cabbage leaves and thus improved rainfastness property.[36,37] However, in the cases of biopesticide formulations, these adjuvants showed very limited rainfastness improvement, which might be due to the weak affinity between biopesticides and latex/starch materials.[37] Moreover, the feasibility of film-forming

adjuvants in cattle pest treatment has not been tested in literature. So far, developing biopesticide formulations with strong adhesion to endure high rainfastness for cattle pest control remains highly desired.

Natural systems with rough surface topologies (eg, viruses, pollen grains) typically exhibit intriguing adhesive properties and high transmission efficiencies.[38,39] For example, pollen grains with numerous spikes on the outer shell (extine) exhibit rough surfaces, which can enable adhesion toward hairy insect legs and mouthparts.[40] Inspired by these natural systems, recently we reported the preparation of mesoporous silica hollow nanospheres with spiky rough surface nanotopography and demonstrated their enhanced adhesion toward bacteria and human embryonic kidney cells for high antibacterial performance and efficient plasmid DNA delivery, respectively.[41,42] Adopting such spiky silica nanoparticles as biopesticides carriers holds great promises for developing nanopesticides with enhanced adhesive property toward cattle hides, contributing to high resistance to withstand rainfall, which has not been reported before. Moreover, the spiky nanotopography would also induce enhanced adhesion between nanopesticides and pest surface, stimulating the potency of contact poison biopesticides (eg, spinosad). To our knowledge, there are rare reports concerning the correlation between adhesive property and pest treatment potency of biopesticides.

In this work, we report the preparation of a new nanospinosad by using spiky silica hollow nanoparticles to load spinosad. This nanospinosad maintained the rough surface topology, and demonstrated an attractive dual adhesion property toward both cattle hides and pest surface (Figure 1A). This unique adhesion behavior has stimulated a high pest mortality for tick treatment on cattle hides and a significantly improved rainfastness property, outperforming the benchmark commercial spinosad product and the nanospinosad formulation using smooth surface silica nanocarriers. This new nanospinosad formulation also exhibited over 10 times higher photostability than the benchmark commercial product in simulating field conditions (Figure 1B), which demonstrated the practical feasibility of our nanospinosad formulation for high performance cattle ectoparasite treatments.

2 | RESULTS AND DISCUSSION

Mesoporous silica hollow nanoparticles with rough surfaces were selected as the spinosad nanocarrier. These rough silica nanoparticles (denoted as RS) with hollow cavity were synthesized using our previously reported

method with slight modifications.[41] They showed uniform particle size of 350 nm and negative surface charge of −28.9 mV (Figures S1 and S2, Table S1). The shells of RS were covered with nanosized silica spikes to form the rough surface morphology, mimicking the surface topology of pollen grains. The hollow structure provided a low particle density for reducing the potential skin penetration, which is important for safe topical products in agricultural applications.[43] Nitrogen sorption analysis indicated that RS possessed ~15 nm mesopores (Figure S3), which can be attributed to the void space between surface spikes. To study the contribution of rough surface, mesoporous silica hollow nanoparticles with smooth surfaces (denoted as SS) were prepared as the comparison material, which possessed similar particle size (330 nm) and negative surface charge property (Figures S1 and S2, Table S1).

A rotary evaporation method was utilized to load spinosad into nanocarriers with the silica: spinosad feeding weight ratio of 7:3 (products denoted as RS-SP and SS-SP, respectively). Field emission scanning electron microscope (FE-SEM) images of RS-SP (Figures 2A and S4A) and SS-SP (Figures 2B and S4B) showed that both RS-SP and SS-SP well maintained the spherical morphology and surface topology after spinosad loading. Without using nanocarriers, pure spinosad (SP) after rotary evaporation formed micron-sized crystals (Figure 2C). Such crystals cannot be observed in the SEM images of RS-SP or SS-SP at different magnifications (Figures 2A,B amd S4), indicating the successful loading of spinosad within silica nanocarriers. Fourier transform infrared (FTIR) spectra of nanospinosads and their nanocarriers are presented in Figure S5. The FTIR spectrum of pure spinosad showed characteristic peaks at 800 to 1200 (C-H out-of-plane bending, C-O stretching), 1369 (CH_3 bending), 1456 (CH_2 bending), 1606 (C=C stretching), 1660 (C=C stretching), 1707 cm^{-1} (C=O stretching), and in range of 2756 to 3023 cm^{-1} (C-H stretching).[44] Most of these peaks can also be clearly observed in the spectra of both RS-SP and SS-SP, further suggesting the complete spinosad loading, while other characteristic peaks at 800 to 1200 cm^{-1} were overlapping with the silica peaks.[45]

The spinosad loading amounts in RS-SP and SS-SP formulations were determined by thermogravimetric analysis (TGA, Figure 2D). Pure spinosad experienced a complete weight loss of 99.9% at around 570°C. Both silica nanocarriers, RS and SS, showed negligible weight loss of ~1.0% to 1.9%, because of the removal of adsorbed moisture and air. Accordingly, the actual spinosad loading contents in RS-SP and SS-SP were calculated to be 31.7% and 29.8%, respectively, which agreed well with the initial feeding ratios. The crystallization feature of spinosad after loading was investigated by differential scanning calorimetry (DSC, Figure 2E). Pure spinosad displayed an endothermic peak at ~130°C, corresponding to the melting point of crystallized spinosad. The physical mixture of spinosad and RS also showed a small endothermic peak at ~120°C, suggesting the existence of spinosad crystals. In contrast, no obvious endothermic peak can be observed in DSC profiles of both RS-SP and SS-SP, indicating the amorphous feature of loaded spinosad. The crystalline nature of spinosad in RS-SP and SS-SP was further examined by X-ray diffraction (XRD) measurements. Comparing to the XRD patterns of pure spinosad and the physical mixture sample, the disappearing of spinosad crystalline peaks in the profiles of both RS-SP and SS-SP further confirmed the amorphous states of spinosad at silica nanocarriers.[46]

In order to investigate the effectiveness and duration of nanospinosad under simulated field conditions, four

FIGURE 1 Schematic representations of the nanospinosad formulation based on rough surface mesoporous silica hollow nanoparticles with, A, strong adhesion to cattle hair and tick larvae and, B, high solar stability and high rainfastness property on cattle hide substrate
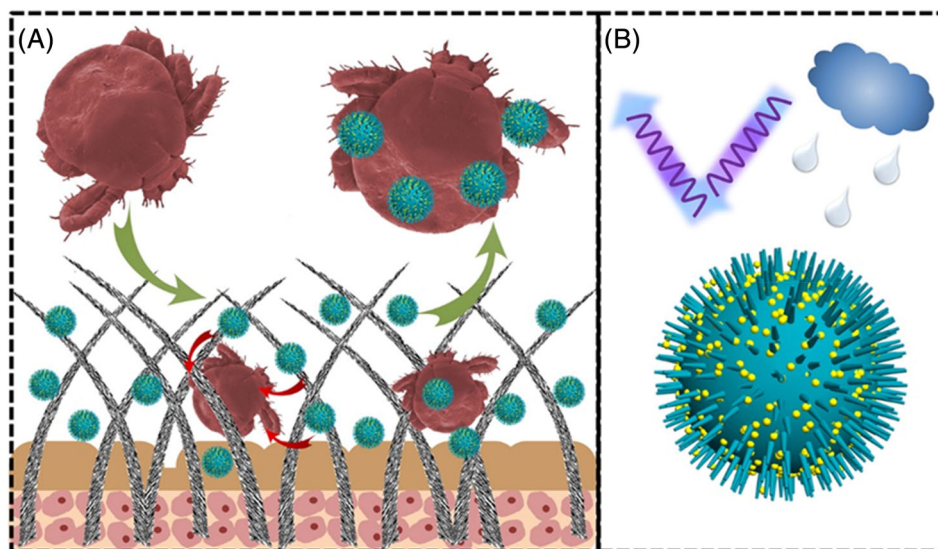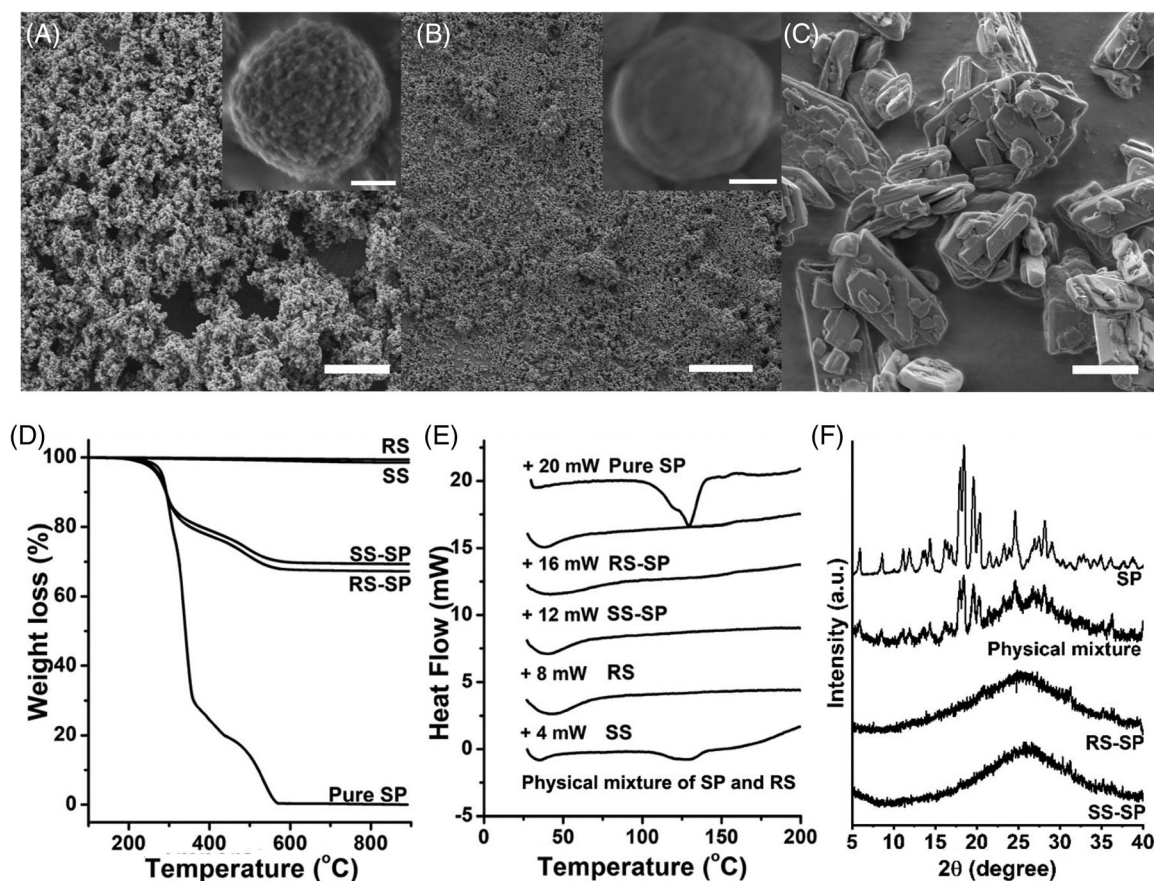
FIGURE 2 Characterization of nanospinosad. Field emission scanning electron microscope (SEM) images of A, RS-SP; B, SS-SP; and, C, pure SP after rotary evaporation. Scale bar: 10 μm. Inset SEM images in A and B are individual RS-SP and SS-SP nanoparticle. Inset scale bar: 100 nm. D, thermogravimetric analysis curves; E, differential scanning calorimetry profiles; and F, X-ray diffraction patterns of RS-SP, SS-SP, pure SP, RS, SS, and the physical mixture of SP and RS

formulations: RS-SP, SS-SP, SP, and commercial product (Extinosad pour-on for sheep, denoted as CP), were prepared and applied on raw cattle hide as substrate for all experiments (see experimental details in supporting information [SI], Figures S6 and S7, Table S2). RS-SP, SS-SP, and CP can be easily formulated in Milli-Q water just by hand-shaking (Figure S7) and the formulations can maintain stable for days, if further treated with ultrasonication. In contrast, pure spinosad needed strong ultrasonication treatment to form an aqueous suspension and would quickly precipitate from it after several minutes, due to the hydrophobic nature of spinosad (Figure S7A).

The tick toxicity of four spinosad formulations was evaluated using a modified tick larvae assay using cattle hair substrate (Figure S8),[47] and the results were summarized in Figures 3A and S9. In general, pure silica nanocarriers showed little contribution to the tick toxicity, and RS-SP demonstrated significantly higher tick toxicity than all other formulations in a wide spinosad concentration (C_S) range (0.1-0.0001 mg/cattle hide

piece). At C_S of 0.1 mg/piece, RS-SP achieved a high tick mortality rate of 100% (Figure 3A), surpassing the performances of SS-SP, CP, and SP (63 ± 8, 35 ± 8, and $25 \pm 3\%$, respectively). When decreasing C_S to 0.01 mg/piece, RS-SP can maintain its tick mortality rate at $74 \pm 1\%$, while the mortality rates of other spinosad formulations had largely decayed to only 27 ± 6 (SS-SP), 11 ± 5 (CP), and $9 \pm 1\%$ (SP). Similar trends can also be observed at ultra-low C_S at 0.001 and 0.0001 mg/piece (-Figure S9), all indicating the advantage of rough surface nanotopography in RS-SP.

To understand the function of rough surface nanotopography, the adhesion amounts of RS-SP and SS-SP on ticks were estimated through measuring the silica contents in treated tick larvae (see experimental details in SI). As shown in Figure 3B, at the initial concentration of 0.1 mg/cattle hide piece, the silica content in RS-SP treated tick larvae was measured to be 0.010 ± 0.001 mg, which was almost 2 times of that in SS-SP treated group (0.0050 ± 0.0001 mg), implying a greatly enhanced adhesion of RS-SP onto tick bodies. Similar result was
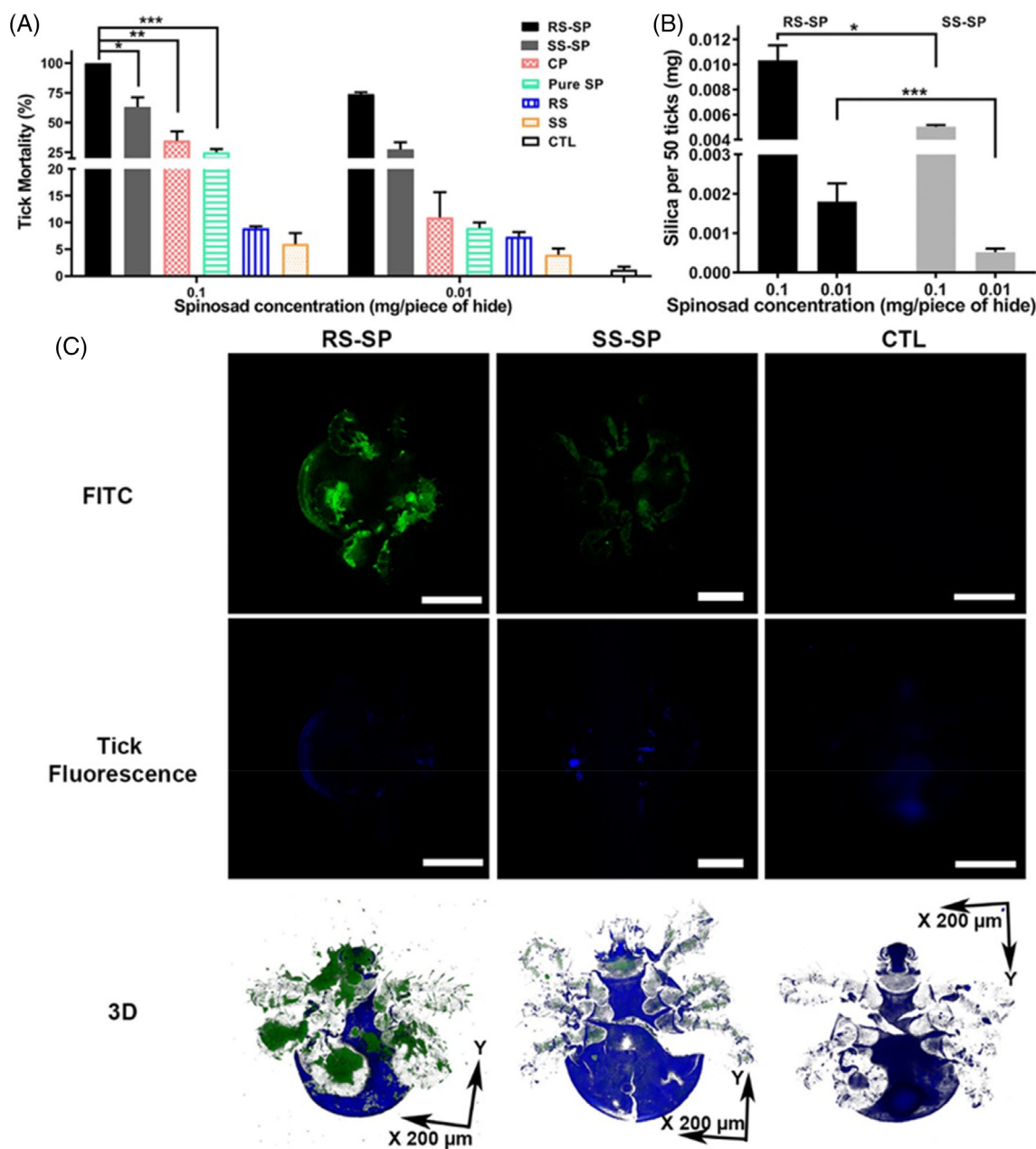
FIGURE 3 Tick larvae toxicity. A, Tick mortality in the tick larvae toxicity assays carried out on cattle hair. B, The silica content on tick larvae after the tick toxicity assays. C, Confocal images and the three-dimensional reconstructions of dead tick larvae from the tick toxicity assays at $C_S = 0.1$ mg/piece of cattle hide (scale bar 200 μm, $z = 0$ in the z stack mode)

obtained at low spinosad concentration (0.01 mg/cattle hide piece), in which RS-SP treated tick larvae showed an over 3 times higher silica content (0.0018 ± 0.0005 mg) than SS-SP group (0.00051 ± 0.00009 mg). These observations demonstrated that the rough surface nanotopography of RS-SP formulation can induce much stronger adhesive capability toward ticks than the counterpart with smooth surface morphology, and consequently lead to greatly enhanced tick toxicity.

The measured silica content in RS-SP treated tick larvae can be also utilized to determine the transfer ratio of

nanospinosad from cattle hair to tick body during the toxicity assays. As described in experimental section and Table S2, 35 mg cattle hair averagely contained 0.01155 mg spinosad and 0.02695 mg RS silica at C_S of 0.1 mg/cattle hide piece, and then interacted with 100 tick larvae. After the toxicity test, the silica content in RS-SP treated tick larvae was measured to be 0.010 ± 0.001 mg per 50 tick larvae, which means that ~74% RS-SP have been transferred from cattle hair to tick bodies (Figure S10). At C_S of 0.01 mg/cattle hide piece, the RS-SP transfer ratio can reach to ~93%. The RS-SP transfer

results reveal that this rough surface nanospinosad formulation has a dual adhesion to both cattle hair and tick body, with the preference of adhering onto ticks for high effectiveness, especially under low concentration treatments.

To further investigate the adhesive property of RS-SP toward ticks, fluorescent confocal microscopy was employed to directly observe the adhesion behavior of RS-SP and compare with SS-SP. Both RS-SP and SS-SP were labeled with fluorescein isothiocyanate (FITC)—a green fluorescent probe. A z-stack mode was used to locate the tick and nanospinosad fluorescence and reconstruct the three-dimensional (3D) fluorescence distribution (see experimental details in SI). When focusing on the ventral surface of a tick ($z = 0$), green fluorescence from FITC-labeled RS-SP and SS-SP can be clearly observed (Figure 3C), indicating the nanospinosads were attached onto tick body surfaces. The confocal image of RS-SP shows much stronger green fluorescence than that of SS-SP, suggesting a higher RS-SP adhering amount, which is consistent with the silica content analysis results (Figure 3B). The weak blue fluorescence observed in RS-SP, SS-SP, and bare tick (control group) can be attributed to the tick autofluorescence. When focusing on the inner body of ticks ($z = 30$, Figure S11), strong blue autofluorescence, but neglectable green fluorescence, was observed in both RS-SP and SS-SP groups, indicating that the nanospinosads dominantly adhered on tick body surfaces rather than being ingested. Therefore, the toxicity of nanospinosads was activated mainly through contact poisoning.[6] The 3D reconstructions of green and blue fluorescence in Figure 3C further confirmed that most nanospinosads were distributed at the surface of tick body and RS-SP exhibited a much higher adhesion content than SS-SP. Moreover, the reconstruction results, especially the RS-SP image, showed that nanospinosads were concentrated in legs, abdomen and mouthparts of a tick.

The distributions of nanospinosads on tick body after the toxicity assays were characterized using FE-SEM (Figures 4 and S12). For RS-SP at C_S of 0.1 mg/piece, a large number of spherical nanoparticles were observed on the tick surface (Figure 4A), depositing on leg hair, abdomen and mouthparts. Reducing C_S to 0.01 mg/piece, many RS-SP nanoparticles can still be observed (Figure 4B), proving the strong adhesive property of RS-SP toward ticks. In contrast, SS-SP at C_S of 0.1 mg/piece only showed several nanoparticles adhering on tick body parts. The SS-SP nanoparticles almost disappeared at C_S of 0.01 mg/piece. These SEM observations further demonstrate the advantage of rough surface nanotopography for inducing enhanced adhesive property to ticks and leading to improved pesticide/pest contact for high toxicity.

In field applications, the effective duration of spinosad applied on cattle is largely affected by weather conditions, especially the rainfall that could remove and dilute spinosad from cattle hide. Other factors such as wind, or cattle's activities/behaviors also would cause spinosad drift or removal. To evaluate the resistance of applied nanospinosads toward these natural factors, the rainfastness test was chosen as a quantitative method. A modified spraying bottle protocol was used to test the rainfastness property of four spinosad formulations including RS-SP, SS-SP, SP, and commercial product (see details in SI, Figure S13).[48] The wash-off amount of silica nanocarriers and the spinosad active components (ie, spinosyn A and spinosyn D) were quantitatively measured using inductively coupled plasma optical emission spectrometry (ICPOES) and electrospray ionization mass spectrometry with multiple reaction mode (ESI-MS-MRM),[49,50] respectively (Figures S14 and S15).

The wash-off amount of silica nanocarriers were compared between RS-SP and SS-SP formulations, and the results were summarized in Figure 5A (the orange bars) and Table S3. Under 2.5 cm artificial rainfall, the silica wash-off amount of RS-SP was measured to be $34.5 \pm 5.8\%$ (Figure 5A). The silica residue left on cattle hide was then calculated to be ~65.5%, which was more than 6 times of SS-SP silica residue (sim;10.1%, Table S3), suggesting a much better rainfastness property of RS-SP than SS-SP. Similar trends were also recorded under other rainfall strengths (Table S3), proving that the rough surface nanotopography of RS-SP can greatly enhance their adhesive capability toward cattle hide and therefore induce highly improved rainfastness property.

The wash-off spinosyns measurements were performed to further study the function of rough surface nanotopography. The wash-off spinosyns contained two parts: spinosyns dissolved in rain water (Figure 5A, blue bars) and spinosyns washed-off with silica nanocarriers (yellow bars). Both two parts were carefully measured by ESI-MS-MRM and then used to calculate the spinosyns residue maintained on cattle hide (see experimental details in SI). Under 2.5 cm artificial rainfall, RS-SP exhibited a relatively low spinosyn A wash-off amount of ~44.8% (Table S4), in which the dissolved spinosyn A was $27.2 \pm 6\%$. Accordingly, the spinosyn A residue maintained on cattle hide for RS-SP was ~55.2%, >5 times of that for SS-SP, >2 times for benchmark commercial product and > 7 times for pure spinosad. The spinosyn D residue content for RS-SP under 2.5 cm rainfall was calculated to be ~62.5%, >8 times of that for SS-SP, >2 times for benchmark commercial product and > 25 times for pure spinosad. The high spinosyn A and D residue contents for RS-SP were recorded under a wide range of rainfall strengths from 0.5 to 2 cm

(Table S4), validating the highest rainfastness property of RS-SP among the four formulations.

FE-SEM was utilized to monitor the adhesion of nanospinosad on cattle hair before and after the rainfastness tests at 2.5 cm artificial rainfall. Figure S16 shows the typical surface morphology of a blank cattle hair composed of overlapping keratin scales. After applying RS-SP formulation onto the raw cattle hide, numerous spherical nanoparticles were distributed rather evenly on hair cuticle (Figure 5B1,B2). The majority of those nanoparticles remained adhering on the hair strand after treated with 2.5 cm rainfall (Figure 5C1,C2), featuring their good adhesive property toward cattle hair. In comparison, SS-SP showed a much lower nanoparticle distribution density on hair cuticle (Figure 5D1,D2) after being applied on the cattle hide piece, and most of those attached nanoparticles were washed away by 2.5 cm rainfall, leaving only a few of them scattered on the cattle hair. This huge difference between RS-SP and SS-SP clearly demonstrates the function of rough surface nanotopography for inducing high adhesion toward cattle hide, which contributes to high resistance toward rainfall and can be extended for withstanding other damaging natural conditions such as wind. The rainfastness study, combined together with the tick surface adhesion study, validate that silica nanoparticles with spiky rough surface nanotopography have a unique dual adhesion function toward both cattle hair and pest surface, leading to high potency and high stability.

The photostability tests of nanospinosads were conducted in natural solar radiation to simulate the field conditions (see experimental details in SI). Figure S17 shows the solar radiation and temperature conditions during the solar stability tests. Cattle hide pieces with four spinosad formulations were divided into three test groups. Group A was placed on rooftop and exposed to
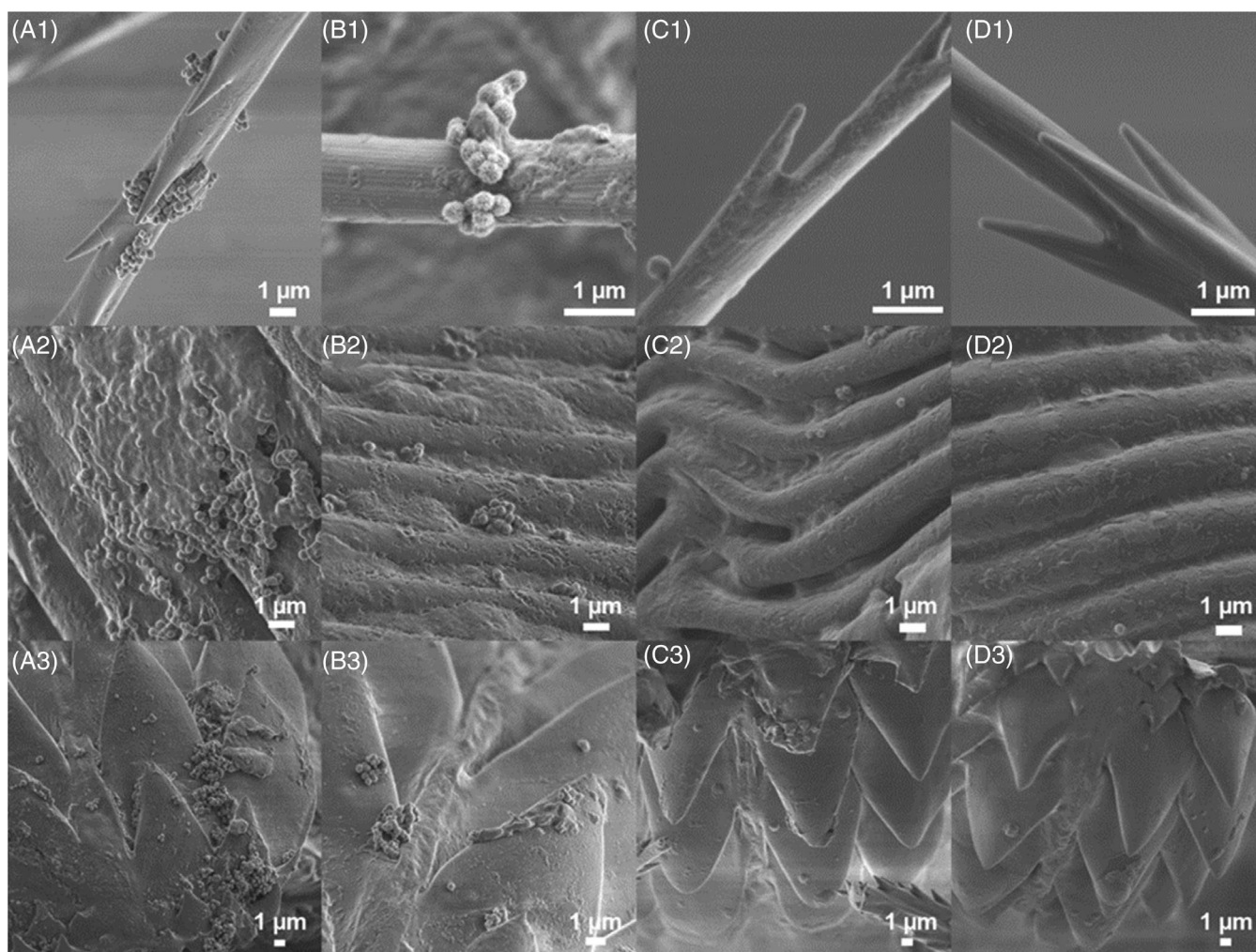

FIGURE 4 Adhesion toward ticks. Field emission scanning electron microscope images of tick larvae treated with RS-SP at, A, 0.1 and B, 0.01 mg/piece of cattle hide, SS-SP at C, 0.1 and D, 0.01 mg/piece of cattle hide in the toxicity assays. 1, leg hair; 2, abdomen; and 3, mouthparts of the dead tick larvae from the toxicity assays

both solar radiation and ambient temperature. Group B was placed on the roof with ambient temperature but covered with aluminum foils to avoid solar radiation. Group C was placed in the lab with constant room temperature of 21°C and protected with aluminum foils.
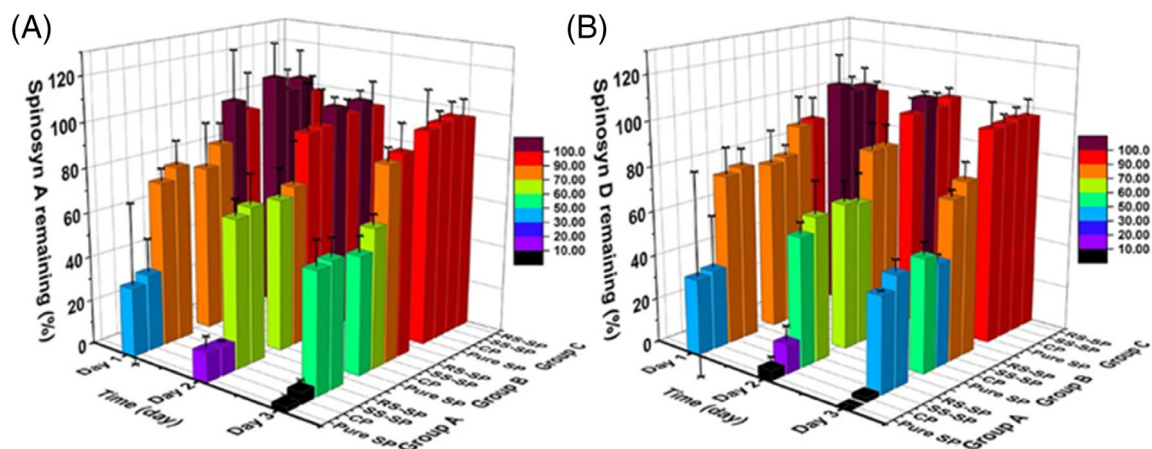
Figure 6 shows the solar stability of spinosyn A and spinosyn D in four formulations applied on cattle hide substrates in three different test groups. In group A and B, all four samples exhibited gradually decreased

spinosyn A and D amount with the time increasing, while no significant spinosyns degradation occurred in group C, suggesting both solar radiation and high temperature would decompose spinosyns. In group A bearing both solar radiation and rooftop ambient temperature, the nanospinosads, that is, RS-SP and SS-SP, have demonstrated greatly improved spinosyns protection than commercial spinosad product and pure spinosad. After 3 days tests, $55 \pm 8\%$ of spinosyn A and $48 \pm 5\%$ of
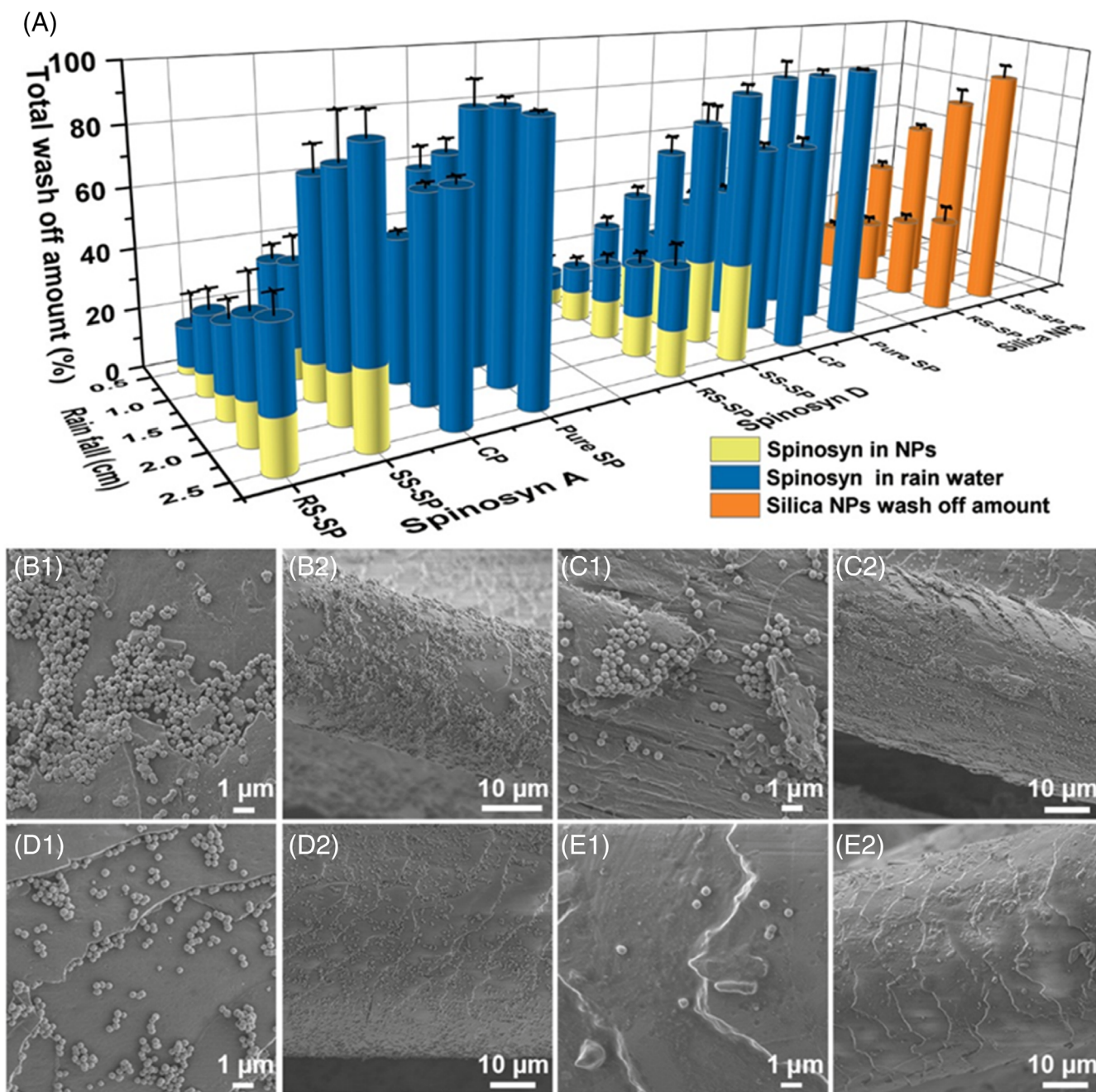
FIGURE 5 Rainfastness tests. A, Washed-off amount of spinosyn A, spinosyn D, and silica from cattle hair in the rainfastness tests. Field emission scanning electron microscope images of cattle hair applied with RS-SP, B, before and, C, after 2.5 cm of rain fall, cattle hair applied with SS-SP, D, before and, E, after 2.5 cm of rain fall. 1, high magnification; and 2, low magnification FE-SEM images

FIGURE 6 Solar stability tests. The photostability of spinosyn A, A, and spinosyn D, B, of four spinosad formulations applied on cattle hide substrates

spinosyn D were maintained in RS-SP applied cattle hide, $53 \pm 9\%$ of spinosyn A and $41 \pm 1\%$ of spinosyn D were maintained in SS-SP case, both showing significant enhancements (>10 times higher) over the commercial product ($5.1 \pm 3.2\%$ spinosyn A, $2.0 \pm 0.6\%$ spinosyn D) and pure spinosad ($2.1 \pm 2.3\%$ spinosyn A, $1.1 \pm 0.7\%$ spinosyn D). The significant differences were confirmed by the *t*-test with $P < .001$ and $P < .0001$ for spinosyn A and spinosyn D, respectively.

In group B with only rooftop ambient temperature, the nanospinosads also exhibited better spinosyns protection than other formulations, although the differences of spinosyns residue amount were less significant ($P < .05$ and $P < .01$ for spinosyn A and spinosyn D, respectively). After 3 days tests, $88 \pm 11\%$ of spinosyn A and $72 \pm 7\%$ of spinosyn D were maintained in RS-SP applied cattle hide, $85 \pm 6\%$ of spinosyn A and $68 \pm 3\%$ of spinosyn D were maintained in SS-SP case, higher than those in commercial product ($60 \pm 4\%$ spinosyn A, $46 \pm 2\%$ spinosyn D) and pure spinosad ($51 \pm 7\%$ spinosyn A, $49 \pm 4\%$ spinosyn D). The solar stability tests revealed that the silica nanocarriers had promising protective functions for photolabile biopesticides. The slightly better protection effect of rough surface nanocarriers over their smooth surface counterparts could be due to their higher porosity that provided more intimate contact between spinosad and siliceous frameworks.

3 | CONCLUSION

In summary, a new nanospinosad was developed by utilizing rough surface silica nanoparticles to immobilize spinosad. This nanospinosad possessed appealing dual adhesion and protection functions, ideal for high

performance cattle ectoparasites controls. When applied on cattle hide for tick treatment, it exhibited high adhesive property toward both tick surface and cattle hair, leading to significantly higher pest mortality and greatly improved resistance against rainfall over the benchmark commercial spinosad product. Furthermore, this nanospinosad also showed attractive photostability that was over10 times higher than that of the commercial product, demonstrating its promising potential as an effective cattle pesticide control formulation under practical field conditions. The novel nanospinosad and its design concept provide new inspirations for the development of high-efficient biopesticides and have the potential to be adopted for manufacturing other products for livestock healthcare.

4 | EXPERIMENTAL SECTION

4.1 | Synthesis of silica nanocarriers

Silica nanoparticles with rough and smooth surface were synthesized according to our previous report[41] with modifications to increase the size. In the synthesis of silica nanocarrier with rough surface (denoted as RS), resorcinol (0.2 g) and formaldehyde (37 wt%, 0.28 mL) were added to the solution composed of ammonia aqueous solution (28 wt%, 3.0 mL), deionized water (10 mL), and ethanol (70 mL). The mixture was vigorously stirred for 6 hours at room temperature, then 0.6 mL of tetraethyl orthosilicate (TEOS, >98%) was added into the solution and stirred for 8 minutes before another addition of resorcinol (0.4 g) and formaldehyde (37 wt%, 0.56 mL). The mixture was stirred for another 2 hours at room temperature, and then the as-synthesized $RF@RF-SiO_2@RF$

composites were collected by centrifugation, ethanol washing and drying at 50°C. Finally, RS were obtained by calcination at 550°C for 5 hours with a temperature ramp rate of 2°C/min in air.

4.2 | Synthesis of nanospinosad

A rotary evaporation method was utilized for encapsulation of spinosad with either RS or SS. In the loading of spinosad, 700 mg of each silica nanocarriers was dispersed in 200 mL ethanol in ultrasonic bath and added to 200 mL spinosad in ethanol solution (1.5 mg/mL) in the dark, with a spinosad to silica feeding ratio of 3:7. The mixture was removed into a long cylindrical flask attached to a rotary evaporator (BUCHI R-210) and evaporated at 40°C in a vacuum system in the dark with a residual pressure of 175 mbar until all solvent had been removed (denoted as RS-SP and SS-SP, respectively). In comparison, similar procedure had been carried out with spinosad-ethanol solution only (pure spinosad).

ORCID
Chengzhong Yu https://orcid.org/0000-0003-3707-0785

REFERENCES
1. Cantrell CL, Dayan FE, Duke SO. Natural products as sources for new pesticides. *J Nat Prod*. 2012;75:1231-1242.
2. Seiber JN, Coats J, Duke SO, Gross AD. Biopesticides: state of the art and future opportunities. *J Agric Food Chem*. 2014;62:11613-11619.
3. Pavela R, Benelli G. Essential oils as ecofriendly biopesticides? Challenges and constraints. *Trends Plant Sci*. 2016;21:1000-1007.
4. Copping LG, Duke SO. Natural products that have been used commercially as crop protection agents. *Pest Manag Sci*. 2007;63:524-554.
5. Thompson GD. Spinosyns: an overview of new natural insect management systems. *Proc. Beltwide Cotton Production Conference, San Antonio, TX*. : ; 1995:1039-1043.
6. Thompson GD, Dutton R, Sparks TC. Spinosad—a case study: an example from a natural products discovery programme. *Pest Manag Sci*. 2000;56:696-702.
7. Kirst HA. The spinosyn family of insecticides: realizing the potential of natural products research. *J Antibiot*. 2010;63:101-111.
8. Breslin WJ, Marty MS, Vedula U, Liberacki AB, Yano BL. Developmental toxicity of Spinosad administered by gavage to CD (R) rats and New Zealand white rabbits. *Food Chem Toxicol*. 2000;38:1103-1112.
9. Bernardo U, Viggiani G. Effects of spinosad, a new insect control agent naturally derived on the mealybug parasitoid *Leptomastix dactylopii* Howard (Hymenoptera: Encyrtidae). *Bull IOBC/WPRS*. 2000;23:81-84.
10. Crouse GD, Sparks TC, Schoonover J, et al. Recent advances in the chemistry of spinosyns. *Pest Manag Sci*. 2001;57:177-185.
11. Tillman PG, Mulrooney JE. Effect of selected insecticides on the natural enemies Coleomegilla maculata and *Hippodamia convergens* (Coleoptera: Coccinellidae), *Geocoris punctipes* (Hemiptera: Lygaeidae), and *Bracon mellitor*, Cardiochiles nigriceps, and Cotesia marginiventris (Hymenoptera: Braconidae) in cotton. *J Econ Entomol*. 2000;93:1638-1643.
12. Boyd ML, Boethel DJ. Residual toxicity of selected insecticides to heteropteran predaceous species (Heteroptera: Lygaeidae, Nabidae, Pentatomidae) on soybean. *Environ Entomol*. 1998;27:154-160.
13. Williams T, Valle J, Vinuela E. Is the naturally derived insecticide Spinosad (R) compatible with insect natural enemies? *Biocontrol Sci Technol*. 2003;13:459-475.
14. Davey RB, Miller JA, George JE, Snydee DE. Effect of repeated spinosad treatments on cattle against Boophilus annulatus under South Texas field conditions. *Southw Entomol*. 2005;30:245-255.
15. Davey RB, George JE, Snyder DE. Efficacy of a single whole-body spray treatment of spinosad, against *Boophilus microplus* (Acari: Ixodidae) on cattle. *Vet Parasitol*. 2001;99:41-52.
16. Kaushik P, Shakil NA, Kumar J, Singh MK, Singh MK, Yadav SK. Development of controlled release formulations of thiram employing amphiphilic polymers and their bioefficacy evaluation in seed quality enhancement studies. *J Environ Sci Health Part B Pestic Contam Agric Wastes*. 2013;48:677-685.
17. Pankaj SNA, Kumar J, Singh MK, Singh K. Bioefficacy evaluation of controlled release formulations based on amphiphilic nano-polymer of carbofuran against Meloidogyne incognita infecting tomato. *J Environ Sci Health Part B Pestic Contam Agric Wastes*. 2012;47:520-528.
18. Xiang CH, Taylor AG, Hinestroza JP, Frey MW. Controlled release of nonionic compounds from poly(lactic acid)/cellulose nanocrystal nanocomposite fibers. *J Appl Polym Sci*. 2013;127:79-86.
19. Nguyen HM, Hwang IC, Park JW, Park HJ. Enhanced payload and photo-protection for pesticides using nanostructured lipid carriers with corn oil as liquid lipid. *J Microencapsul*. 2012;29:596-604.
20. Nguyen HM, Hwang IC, Park JW, Park HJ. Photoprotection for deltamethrin using chitosan-coated beeswax solid lipid nanoparticles. *Pest Manag Sci*. 2012;68:1062-1068.
21. Kah M, Beulke S, Tiede K, Hofmann T. Nanopesticides: state of knowledge, environmental fate, and exposure modeling. *Crit Rev Environ Sci Technol*. 2013;43:1823-1867.
22. Kah M, Kookana RS, Gogos A, Bucheli TD. A critical evaluation of nanopesticides and nanofertilizers against their conventional analogues. *Nat Nanotechnol*. 2018;13:677-684.
23. Kah M, Hofmann T. Nanopesticide research: current trends and future priorities. *Environ Int*. 2014;63:224-235.

24. Xu C, Lei C, Yu CZ. Mesoporous silica nanoparticles for protein protection and delivery. *Front Chem*. 2019;7:12.

25. Chen Y, Chen HR, Shi JL. In vivo bio-safety evaluations and diagnostic/therapeutic applications of chemically designed mesoporous silica nanoparticles. *Adv Mater*. 2013;25:3144-3176.

26. Wibowo D, Zhao C-X, Peters BC, Middelberg APJ. Sustained release of fipronil insecticide in vitro and in vivo from biocompatible silica nanocapsules. *J Agric Food Chem*. 2014;62:12504-12511.

27. Song M-R, Cui S-M, Gao F, et al. Dispersible silica nanoparticles as carrier for enhanced bioactivity of chlorfenapyr. *J Pestic Sci*. 2012;37:258-260.

28. Li Z-Z, Chen J-F, Liu F, et al. Study of UV-shielding properties of novel porous hollow silica nanoparticle carriers for avermectin. *Pest Manag Sci*. 2007;63:241-246.

29. Cao L, Zhou Z, Niu S, et al. Positive-charge functionalized mesoporous silica nanoparticles as nanocarriers for controlled 2,4-dichlorophenoxy acetic acid sodium salt release. *J Agric Food Chem*. 2018;66:6594-6603.

30. Ao M, Zhu Y, He S, et al. Preparation and characterization of 1-naphthylacetic acid-silica conjugated nanospheres for enhancement of controlled-release performance. *Nanotechnology*. 2013;24:035601.

31. Huang BB, Zhang SF, Chen PH, Wu G. Release and degradation of microencapsulated spinosad and emamectin benzoate. *Sci Rep*. 2017;7:10.

32. Davey RB, Miller JA, Miller RJ, George JE. Effect of rainfall exposure immediately after a single dip treatment with Coumaphos on the control of Rhipicephalus (Boophilus) microplus (Acari: Ixodidae) on infested cattle. *J Med Entomol*. 2009;46:93-99.

33. Pinero JC, Mau RFL, McQuate GT, Vargas RI. Novel bait stations for attract-and-kill of pestiferous fruit flies. *Entomol Exp Appl*. 2009;133:208-216.

34. Bylemans D, Schoonejans T. Spinosad, a useful tool for insect control in top fruit. *Bcpc Conference: Pests & Diseases 2000, Proceedings*. Vol 1–3. Farnham: British Crop Protection Council; 2000:33-40.

35. Hulbert D, Isaacs R, Vandervoort C, Wise JC. Rainfastness and residual activity of insecticides to control Japanese beetle (Coleoptera: Scarabaeidae) in grapes. *J Econ Entomol*. 2011; 104:1656-1664.

36. Thacker JRM, Young RDF. The effects of six adjuvants on the rainfastness of chlorpyrifos formulated as an emulsifiable concentrate. *Pestic Sci*. 1999;55:198-200.

37. McGuire MR, Shasha BS, Eastman CE, OloumiSadeghi H. Starch- and flour-based sprayable formulations: effect on rainfastness and solar stability of *Bacillus thuringiensis*. *J Econ Entomol*. 1996;89:863-869.

38. Zhu P, Liu J, Bess J Jr, et al. Distribution and three-dimensional structure of AIDS virus envelope spikes. *Nature*. 2006;441:847-852.

39. Barrier S, Diego-Taboada A, Thomasson MJ, et al. Viability of plant spore exine capsules for microencapsulation. *J Mater Chem*. 2011;21:975-981.

40. Thorp RW. The collection of pollen by bees. *Plant Syst Evol*. 2000;222:211-223.

41. Song H, Nor YA, Yu MH, et al. Silica nanopollens enhance adhesion for long-term bacterial inhibition. *J Am Chem Soc*. 2016;138:6455-6462.

42. Song H, Yu MH, Lu Y, et al. Plasmid DNA delivery: nanotopography matters. *J Am Chem Soc*. 2017;139:18247-18254.

43. Zhang J, Raphael AP, Yang YN, Popat A, Prow TW, Yu CZ. Nanodispersed UV blockers in skin-friendly silica vesicles with superior UV-attenuating efficiency. *J Mater Chem B*. 2014;2: 7673-7678.

44. El Badawy M, Taktak NEM, Awad OM, Elfiki SA, Abou El-Ela NE. Evaluation of released malathion and spinosad from chitosan/alginate/gelatin capsules against *Culex pipiens* larvae. *Res Rep Trop Med*. 2016;7:23-38.

45. Mahadik DB, Rao AV, Rao AP, Wagh PB, Ingale SV, Gupta SC. Effect of concentration of trimethylchlorosilane (TMCS) and hexamethyldisilazane (HMDZ) silylating agents on surface free energy of silica aerogels. *J Colloid Interface Sci*. 2011;356:298-302.

46. Juère E, Kleitz F. On the nanopore confinement of therapeutic drugs into mesoporous silica materials and its implications. *Microporous Mesoporous Mater*. 2018;270:109-199.

47. Miller RJ, Davey RB, George JE. Modification of the food and agriculture organization larval packet test to measure Amitraz-susceptibility against Ixodidae. *J Med Entomol*. 2002;39: 645-651.

48. Lopez BB, Hua TQ. Evaluation of the rain fastness of pesticide formulations using simulated leaf surfaces with a visual rating system. In: Collins HM, Hall FR, Hopkinson M, eds. *Pesticide Formulations and Application Systems: 15th Volume*. Vol 1268. W Conshohocken: American Society Testing and Materials; 1996:182-192.

49. Morales A, Ruiz I, Oliva J, Barba A. Determination of sixteen pesticides in peppers using high-performance liquid chromatography/mass spectrometry. *J Environ Sci Health Part B Pestic Contam Agric Wastes*. 2011;46:525-529.

50. Sannino A. Determination of three natural pesticides in processed fruit and vegetables using high-performance liquid chromatography/tandem mass spectrometry. *Rapid Commun Mass Spectrom*. 2007;21:2079-2086.

SUPPORTING INFORMATION

Additional supporting information may be found online in the Supporting Information section at the end of this article.